Nuclear Engineering and Technology 55 (2023) 3417–3422

Contents lists available at ScienceDirect

Nuclear Engineering and Technology

journal homepage: www.elsevier.com/locate/net

Original Article

Real-time monitoring of ultra-high dose rate electron beams using bremsstrahlung photons

Hyun Kim, Dong Hyeok Jeong, Sang Koo Kang, Manwoo Lee, Heuijin Lim, Sang Jin Lee, Kyoung Won Jang*

Research Center, Dongnam Institute of Radiological & Medical Sciences, Busan, 46033, South Korea

ARTICLE INFO

Article history:
Received 1 July 2022
Received in revised form
9 December 2022
Accepted 30 May 2023
Available online 13 July 2023

Keywords:
UHDR electron Beams
Real-time monitoring
Ionization chamber
FLASH radiotherapy

ABSTRACT

Recently, as the clinically positive biological effects of ultra-high dose rate (UHDR) radiation beams have been revealed, interest in flash radiation therapy has increased. Generally, FLASH preclinical experiments are performed using UHDR electron beams generated by linear accelerators. Real-time monitoring of UHDR beams is required to deliver the correct dose to a sample. However, it is difficult to use typical transmission-type ionization chambers for primary beam monitoring because there is no suitable electrometer capable of reading high pulsed currents, and collection efficiency is drastically reduced in pulsed radiation beams with ultra-high doses. In this study, a monitoring method using bremsstrahlung photons generated by irradiation devices and a water phantom was proposed. Charges collected in an ionization chamber located at the back of a water phantom were analyzed using the bremsstrahlung tail on electron depth dose curves obtained using radiochromic films. The dose conversion factor for converting a monitored charge into a delivered dose was determined analytically for the Advanced Markus® chamber and compared with experimentally determined values. It is anticipated that the method proposed in this study can be useful for monitoring sample doses in UHDR electron beam irradiation.

1. Introduction

In conventional radiation therapy (RT), dose rates of several Gy/min are typically used, whereas ultra-high dose rates (UHDRs) of over 40 Gy/s are used in FLASH RT (FRT) [1–3]. The biological mechanism for the increase in tolerance dose of normal tissues by irradiation with UHDR FLASH beams is still unclear [2], and FRT devices for patient treatment have not yet been commercialized. Preclinical experiments using cells and small animals are currently conducted using modified medical linear accelerators (LINACs) or research LINACs to generate UHDR FLASH beams [4–6]. The reported dose rates from experimental devices worldwide are 40–1000 Gy/s, which is 1200–30000 times higher than that of conventional RT [4–7].

Monitoring UHDR beams using existing dosimeters is challenging. Several dosimeters, such as radiochromic films, glass, and alanine dosimeters, can be used in the dosimetry of UHDR beams; however, they are time-consuming processes that prevent real-time monitoring. Application of clinical ionization chambers, which are used for reference dosimetry in conventional RT, is difficult for real-time monitoring of UHDR beams because of the decrease in the collection efficiency. According to Petersson et al., the ion collection efficiency of the Advanced Markus® chamber (PTW, Germany) is close to 100% at a dose per pulse (DPP) below 50 mGy but rapidly decreases to approximately 85% at a DPP of approximately 400 mGy [8]. As the DPPs used in FRT studies are higher than 400 mGy, the collection efficiency of the ionization chambers will be very low in FRT studies. Boag et al. published theoretical models to correct the collection efficiency of the ionization chamber at high dose rates [9], and Laitano et al. confirmed that the Boag models work up to approximately 120-mGy DPP [10]. Recently, Jeong et al. proposed a fitting formula based on the Boag model up to approximately 115-mGy DPP [11]; thus far, no correction method for higher DPPs has been reported. However, these methods have limitations in real-time beam monitoring because they are based on two-voltage analysis [10]. In addition, the transmission-type ionization chambers for beam monitoring used in medical LINACs are difficult to apply to ultra-high-dose pulsed radiation beams due to the lack of suitable electrometers capable of reading very high pulsed currents. Therefore, real-time

* Corresponding author.
E-mail address: kko988@dirams.re.kr (K.W. Jang).

https://doi.org/10.1016/j.net.2023.05.033

beam monitoring using ionization chambers for UHDR beams may cause significant errors. Nonetheless, if the dose rate is sufficiently reduced without affecting the primary beams where the ionization chamber is located, the chamber can be used for beam monitoring; here, the primary beams are radiation beams incident on targets or phantoms and the position of the ionization chamber can be outside of a phantom.

Meanwhile, according to Zhu et al., bremsstrahlung photons are produced by the interaction of electrons in the LINAC head, lead block, and water phantom and depend on the electron energy and field size [12]. The reported doses for the bremsstrahlung photons in 6–22 MeV medical accelerators were less than 2% of the maximum dose in the phantom [12].

In this study, we measured bremsstrahlung photons with an ionization chamber attached to the back of a water phantom for real-time monitoring of UHDR beams, using a prototype FLASH irradiator based on the compact LINAC developed at the Dongnam Institute of Radiological and Medical Sciences [7]. The relationship between the measured charge from the ionization chamber attached to the back of the phantom and the maximum dose of the primary electron beam in the phantom was analyzed. The charge as a function of the maximum dose was derived using an exponential function containing an empirically determined attenuation coefficient using the measured photon tail. The dose conversion factor (DCF) for converting a monitored charge into a delivered dose to the sample was determined analytically and compared to experimental results using the Advanced Markus® chamber.

2. Materials and methods

2.1. Bremsstrahlung photons

Electrons lose their energy by interacting with atomic electrons and nuclei in the medium, and the total energy loss of electrons through the medium is the sum of the collisional and radiative losses. The radiative losses are mostly due to the bremsstrahlung effect of electrons. The total radiative energy is expressed as the radiation yield (Y) [13].

$$Y = \frac{1}{E_0}\int_0^{E_0} \frac{S_{rad}(E,Z)}{S_{tot}} dE \tag{1}$$

where E_0 is the initial electron energy, S_{tot} and S_{rad} are the total and radiative stopping powers, respectively. The Y depends on the energy and atomic number of the medium. According to the National Institute of Standards and Technology (NIST) data, the values of Y are 0.0035, 0.0191, and 0.0407 for 1-, 5-, and 10-MeV initial electron energies in water, respectively [14]. Thus a 5-MeV electron can produce photons with a total energy of 95 keV until it stops in water. As many photons with a continuous energy spectrum can be emitted in all electron paths, the energy of most photons will be within a few tens of keV. Most of photons will be absorbed by the photoelectric effect and contribute to medium dose, and some will be emitted out of the medium. These events were proportional to the intensity of the primary electron beam. In other words, the number of bremsstrahlung photons produced was proportional to the dose rate of the electron beams.

The irradiation head used in this study consisted of a scattering foil and collimator. The electron pencil beams emitted from the LINAC beam window were scattered through some foils to produce electron beams with a wide and uniform field. Here, the collimator could adjust the field size. The design and structure of the head were described in our previous work [15]. The electron beams emitted from the head were incident on a water phantom containing the target samples to be irradiated. The bremsstrahlung photons could also be produced in both the irradiation head and the phantom by interaction with electron beams.

2.2. Analysis of bremsstrahlung photon tail

To describe the doses induced by bremsstrahlung photons, the doses according to water depth were analyzed. The percentage depth dose (PDD) curve in water for electron beams is shown in Fig. 1, where d_{100} is the depth of the dose maximum, d_{50} is the half-value depth, and d_p is the practical range. These values were applied to determine the reference dose to water for conventional electron beams according to the IAEA TRS-398 dosimetry protocol [16]. d_x is the depth at which the photon dose tail begins and $PDD_x(d_x)$ is the percentage depth dose at d_x. $PDD_x(0)$ is the percentage depth dose at the phantom surface ($d = 0$) obtained by extrapolating the photon dose tail. $PDD_x(0)$ is an assumed value as a surface dose for bremsstrahlung photons, but is useful for predicting doses deeper than d_x.

If we assume that the photon beams attenuate exponentially in a medium, and $\overline{\mu}$ (average linear attenuation coefficient) in the bremsstrahlung tail is properly determined, then the dose by photons at an arbitrary depth can be given as follows:

$$D_x(d) = D_{100}\frac{PDD_x(0)}{100}e^{-\overline{\mu}d} \tag{2}$$

where D_{100} is the dose at depth d_{100}. D_{100} is the reference dose to the sample, which can be determined using film dosimetry. If the ionization chamber is located far from the phantom, the $1/r^2$ factor can be applied in Eq. (2), however it is currently not considered because the chamber is attached to the back of the phantom.

If an ionization chamber is positioned at a depth d_c greater than d_x as shown in Fig. 2, and assuming that electron equilibrium condition is satisfied, the dose (D_{cav}) to chamber cavity is given as follows [17]:

$$D_{cav}(d_c) = D_x(d_c)\left(\frac{\overline{\mu}_{en}}{\rho}\right)_{water}^{air} \tag{3}$$

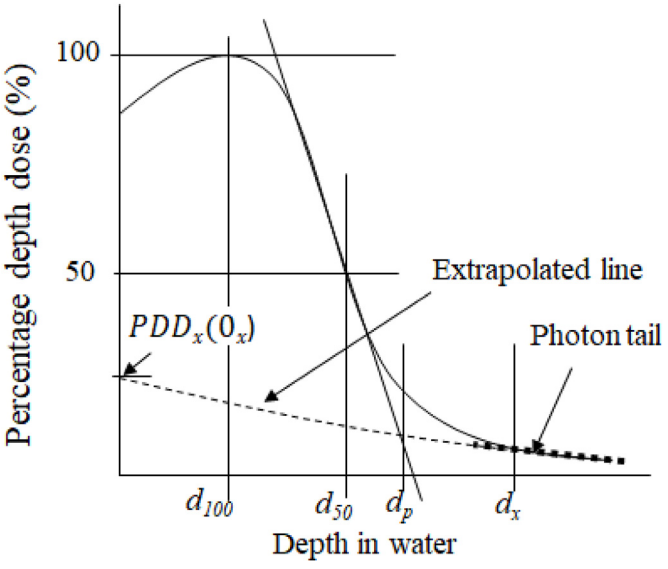

Fig. 1. Analysis of a PDD curve for electron beams in water.

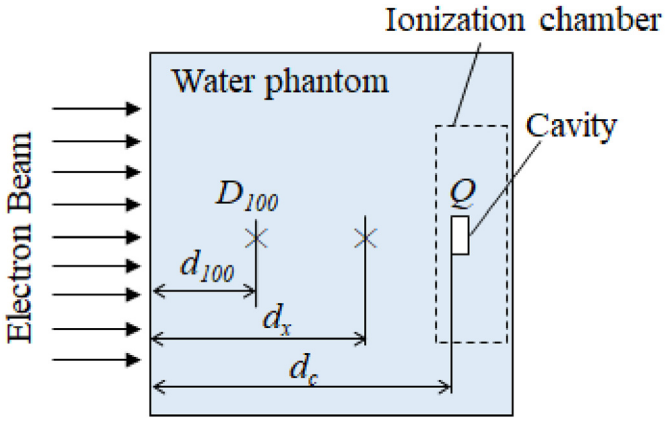

Fig. 2. Analysis of charge produced in air cavity located at d_c.

where $\left(\frac{\bar{\mu}_{en}}{\rho}\right)^{air}_{water}$ is the ratio of the average mass energy absorption coefficient of air to that of water for the photons; since the photon tail consists of tens of keV photons and can be considered as a dose by very low energy electrons, the electron equilibrium condition can be satisfied. Then, the produced charge (dQ) per unit mass (dm) at a point in the chamber cavity is given as follows [17]:

$$\frac{dQ}{dm} = \frac{D_{cav}(d_c)}{(\overline{W}/_e)} \tag{4}$$

where $(\overline{W}/_e)$ is the average energy required to produce an ion pair in air [17]. Assuming that the cavity is small and the photon fluence is uniform throughout the cavity, the total charge (Q) produced in the cavity is given as follows:

$$Q = (\rho V)_{cav}\frac{dQ}{dm} \tag{5}$$

where $(\rho V)_{cav}$ is the mass of the cavity as a product of its density (ρ) and volume (V).

Through these processes, the charge in the cavity can be estimated. If the produced charge can be properly measured using an external electrometer, real-time monitoring of the irradiated dose is possible.

From Eqs. (1)–(5), the charge ($Q(d_c)$) in the cavity shown in Fig. 2 can be expressed as follows:

$$Q(d_c) = D(d_{100})\frac{PDD_x(0)}{100}e^{-\bar{\mu}d_c}\left(\frac{\bar{\mu}_{en}}{\rho}\right)^{air}_{water}\frac{(\rho V)_{cav}}{(\overline{W}/_e)} \tag{6}$$

Therefore, the DCF for converting the measured charge to the maximum dose can be defined as the ratio of $D(d_{100})$ to $Q(d_c)$. The analytically calculated DCF (DCF_{cal}) using Eq. (6) is expressed as follows:

$$DCF_{cal} = \frac{D(d_{100})}{Q(d_c)} = \left[\frac{PDD_x(0)}{100}e^{-\bar{\mu}d_c}\left(\frac{\bar{\mu}_{en}}{\rho}\right)^{air}_{water}\frac{(\rho V)_{cav}}{(\overline{W}/_e)}\right]^{-1} \tag{7}$$

In Eq. (7), DCF has constant values under the same irradiation geometry. Eq. (7) is the DCF derived using the analytical method and compared with the experimentally determined values. If the DCF is properly determined, the irradiated dose can be determined by monitoring the charge using an ionization chamber. $\bar{\mu}$ was determined by exponential fitting to the photon tail measured by film dosimetry, and $\left(\frac{\bar{\mu}_{en}}{\rho}\right)^{air}_{water}$ can be obtained from the effective photon energy determined by the $\bar{\mu}$. In this study, we used the photon cross-section database supported by NIST [14].

2.3. Measurements

The ionization chamber used for the measurements was an Advanced Markus® chamber (PTW, Germany). The chamber provides a high electric field with an electrode spacing of 0.1 cm and high spatial resolution with a cavity volume of 0.02 cm^3; which is widely used in precise electron beam dosimetry. To obtain the cavity charge, the electrometer used throughout this study was UNIDOS^{WEBLINE}® (PTW, Germany). The air density for charges (Q_{raw}) measured in the chamber was corrected using the temperature (T) and atmospheric pressure (P) as follows:

$$Q_{cor} = Q_{raw}\frac{P_0}{P}\left(\frac{273.16+T}{273.16+T_0}\right) \tag{9}$$

where T_0 and P_0 are the normal temperature (20 °C) and pressure (101.325 kPa), respectively. The ionization chamber was attached behind a small water phantom and covered with a 1.5-cm-thick polymethyl methacrylate block to minimize scattered radiation from the surroundings; therefore, the effect of scattered radiation from the surroundings was not considered in this study.

A small plastic tube with a 1-cm diameter and a 4-cm height was mounted on the phantom with external dimensions of 5.5 × 5.5 × 5.0 cm^3. A liquid culture medium containing the cells and agar was contained in the cell tube; it is assumed that the medium interacts with the electron beams with the same characteristics as water.

The source-to-surface distance (SSD) was 20 cm, where the source refers to the first scattering foil on the irradiation head. And the field diameter delivering 90% dose of the center dose of the field was 5 cm at the SSD. In our LINAC system, it was possible to control the number of irradiation pulses in the range of pulse repetition rates up to 200 Hz. The DPP at the maximum dose depth in the phantom was approximately 2.2 Gy; therefore, the expected dose rate was close to 330 Gy/s for a pulse repetition rate of 150 Hz. The detailed structure and operation of the LINAC and the irradiation head structure have been described in our previous work [7,15]. The overall geometry of this measurement and the experimental set-up are shown in Figs. 3 and 4, respectively.

The maximum dose, D_{100} in Eq. (2) as a reference dose for cell irradiation was determined by film dosimetry in the phantom. Two types of radiochromic film, GAFchromic™ EBT3 and GAFchromic™ MD-V3 (Ashland, US), supporting dose ranges up to 10 and 100 Gy respectively, were used for film dosimetry. Film calibration was performed under the condition of SSD = 80 cm and dose rate 11.8 Gy/min for electron beam, and the Advanced Markus®

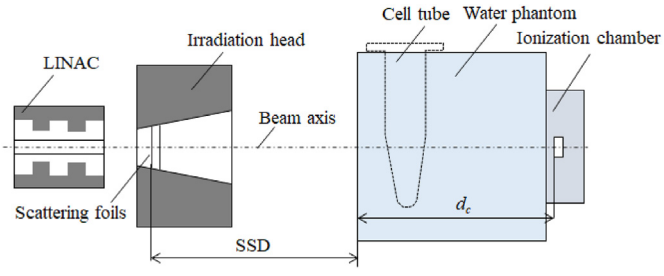

Fig. 3. Irradiation geometry of the charge measurement.

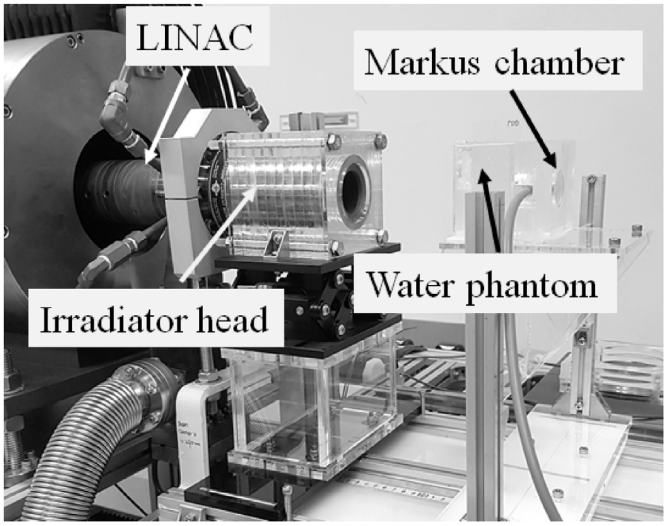

Fig. 4. Experimental setup of charge measurement for beam monitoring.

chamber (PTW, Germany) calibrated for absorbed dose to water for Co-60 gamma rays at the standard laboratory was used for measured the dose to the film position. The TRS-398 dosimetry protocol was applied for the dose determination [16]. For film calibration, 1.07, 2.04, 4.13, 5.63, and 8.73 Gy for GAFchromic™ EBT3, and 4.73, 10.14, 19.63, 27.53, 45.43, 63.34, and 90.03 Gy for GAFchromic™ MD-V3 film were irradiated to each pieces of film. The irradiated films were analyzed using the 10000XL™ flatbed scanner (Epson, US) and filmQApro™ software (Ashland, US) were used for analysis. The estimated uncertainty in Advanced Markus® chamber dosimetry is 2.3%, and it is difficult to analyze the total uncertainty including film measurement. It was estimated to be about 5% according to a study by Elsa et al. [18] and current study is expected to be similar.

The relationship between the number of pulses and reference doses was determined by the irradiation of films whose position was the same as that of the tube in the phantom. For several beam pulses, such as 5, 10, 15, 20, 30, and 40, the experimental DCF (DCF_{mea}) in Eq. (10) was determined by using the simultaneously obtained outputs of the chamber and the films, which are the corrected charges (Q_{cor}) in Eq. (9) and the measured dose (D_{mea}), respectively.

$$DCF_{mea} = \frac{D_{mea}}{Q_{cor}} \tag{10}$$

The depth-dose curve can be measured through a single irradiation of the film inserted horizontal to the electron beams in the phantom. In this study, the electron PDD was obtained by irradiating 40 beam pulses (approximately 89 Gy at the maximum dose depth [d_{100}]) onto the GAFchromic™ MD-V3 film in water. As the dose at the photon tail region was approximately 0.2% (approximately 0.18 Gy) of the maximum dose (D_{100}), which was too low to accurately analyze the photon tail, the GAFchromic™ EBT3 (Ashland, US) film sensitive to low-dose analysis within 10 Gy was additionally used for the photon tail measurements. Eventually, doses of 0.5 and 1 Gy were delivered to the photon tail region by irradiation with 255 beam pulses (approximately 565 Gy at the maximum dose depth). In this case, the front part of the depth-dose curve was saturated, but the doses in the photon tail region could be properly analyzed. The photon tail determined using the above method was used to obtain the physical parameters of Eq. (7) for the theoretical DCF calculations.

3. Results

Fig. 5 shows the irradiated films. Fig. 5(a) shows the GAFchromic™ MD-V3 film irradiated with 40 pulses to obtain a depth dose for primary electron beams, and Fig. 5(b) shows the GAFchromic™ EBT3 film irradiated with 255 pulses to obtain a photon tail. The maximum doses delivered to each film were approximately 89 Gy and 565 Gy, respectively; since 89 Gy was measured at 40 pulses using the MD-V3 film, a 2.225 Gy/pulse relationship can be obtained and the delivered dose at 255 pulses on the EBT3 film was 565 Gy.

Fig. 6 shows the doses of the photon tail on the depth-dose curve and the exponential fitting. The final PDD curves obtained for the two types of films are shown in Fig. 7. In the PDD curve, a logarithmic scale on the vertical axis was used to account for the photon tail, and the maximum dose depth (d_{100}) at which the irradiated sample was positioned was approximately 1 cm. The average electron beam energy incident on the phantom is estimated to be about 4.54 MeV from the d_{50} value. As shown in Fig. 6, the average linear attenuation coefficient ($\overline{\mu}$) and photon dose ($PDD_x(0)$) at the surface, obtained by fitting the photon tail, were 0.211 cm^{-1} and 0.341%, respectively. The effective photon energy estimated from the $\overline{\mu}$ was 57.2 keV, and the $\left(\frac{\overline{\mu}_{en}}{\rho}\right)^{air}_{water}$ was 0.9582. As previously mentioned, the NIST database was used in this calculation. As a result, DCF_{cal} was theoretically determined using Eq. (7) is 1.268 Gy/pC.

The results of the relationship between charge and measured dose are shown in Fig. 8, where the doses were measured with the films for 5-, 10-, 15-, 20-, 30-, and 40-pulse irradiations. From these results, the ratio of charge to dose for each measurement was equal to the DCF_{mea} described in Eq. (10). As a result, the DCF_{mea} values were between 1.244 Gy/pC and 1.364 Gy/pC, the mean value and standard deviation were 1.316 Gy/pC and 0.056, respectively.

4. Discussion

In this study, a method for measuring bremsstrahlung photons with an ionization chamber was introduced to monitor UHDR electron beams that are difficult to measure directly. The charge measured at the back of the phantom was theoretically derived as a function of the maximum dose by analyzing the photon tail of the depth-dose curve for the electron beams. To properly analyze the photon tail, a technique of irradiating a low-dose range film with a high dose was applied.

To monitor the delivered dose to the target sample by measuring the charge, the dose conversion coefficient DCF was

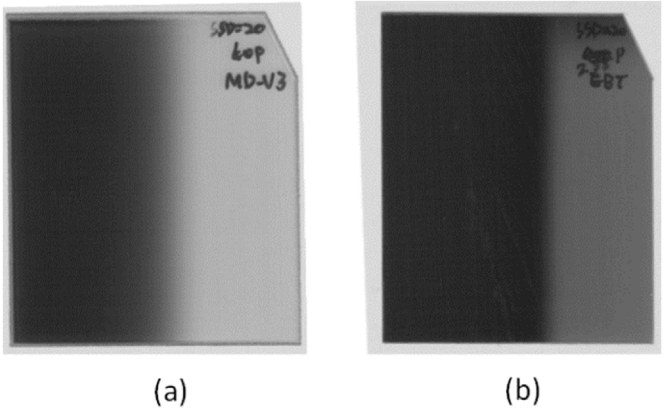

Fig. 5. The irradiated films for the analysis of electron beam depth dose and photon tail.

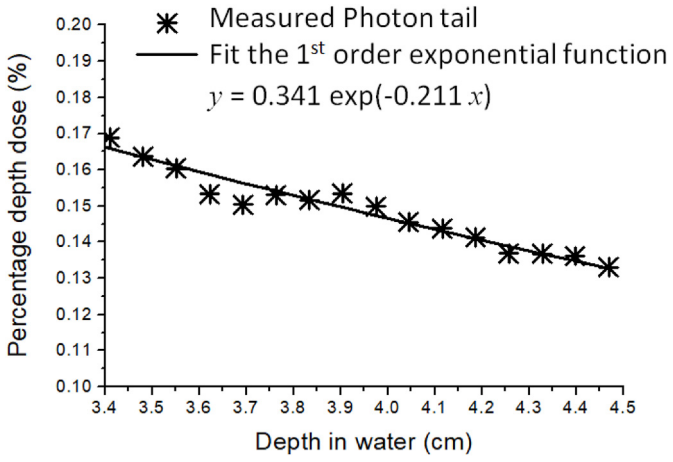

Fig. 6. The fitting of photon dose values at the percentage depth dose.

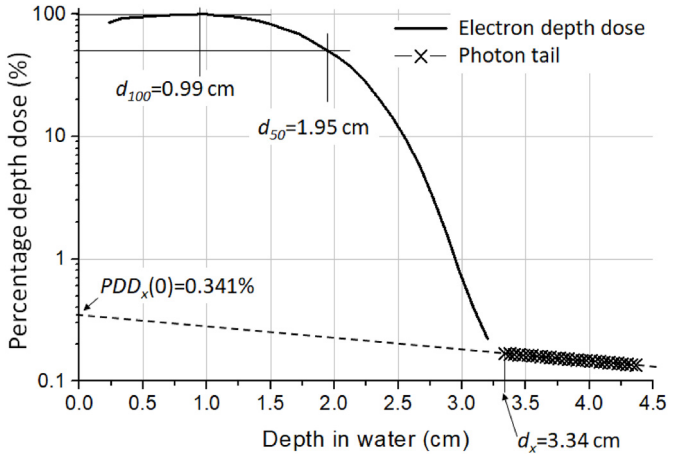

Fig. 7. Percentage depth dose (PDD) curve obtained with two films.

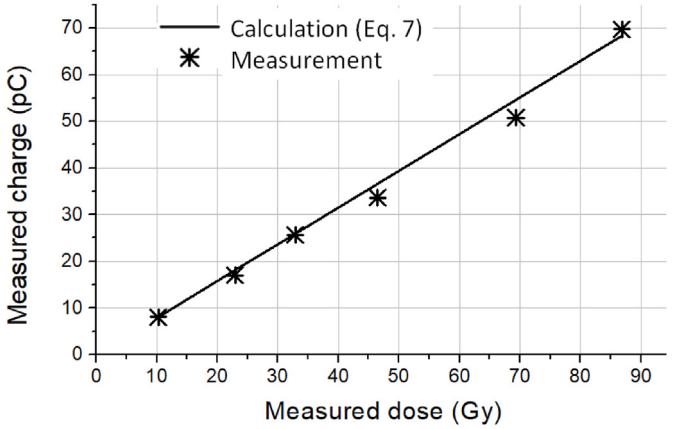

Fig. 8. Calculated and measured charges for measured maximum dose.

introduced, and the theoretically predicted and experimentally determined values were found to be approximately consistent. The measured average DCF was 3.8% higher than the theoretically calculated value. This difference can occur because of the assumption of an ideal ionization chamber with only a cavity, ignoring the plastic body of the chamber. However, it is important to note that the charge measured at a position independent of the primary beam can be analyzed dosimetrically. Therefore, our results can be applied to beam monitoring studies of UHDR irradiation of biological samples. As the DCF is derived from bremsstrahlung photons generated from the interactions of electrons with matter, it depends on the energy of the electron beams. In this regard, it is important to control the LINAC such that the beams generated from the LINAC have energy constancy.

Future research will be conducted to clarify the dependence of DCF including electron beam energy will be required. The Advanced Markus® chamber with a cavity volume of 0.02 cm^3 was used throughout this study, and other ionization chambers can also be used for DCF dependency studies. The chamber must be properly shielded against ambient radiation scattered from the walls, particularly in the case of cylindrical ionization chambers.

5. Conclusion

In this study, a method was proposed for monitoring UHDR electron beams without affecting the primary beam using bremsstrahlung photons. The relationship between the measured charge and the delivered dose was analyzed using the photon tail on the depth-dose curve and was experimentally verified. As analysis of the monitored charges for doses at the photon tail region is possible through this research, it is expected that monitoring techniques for UHDR electron beams can be improved.

Declaration of competing interest

The authors declare that they have no known competing financial interests or personal relationships that could have appeared to influence the work reported in this paper.

Acknowledgment

This work was supported by the Dongnam Institute of Radiological & Medical Sciences (DIRAMS) grant funded by the Korea government (MSIT) (No. 50493-2023)

References

[1] V. Favaudon, L. Caplier, V. Monceau, F. Pouzoulet, M. Sayarath, C. Fouillade, M.-F. Poupon, I. Brito, P. Hupé, J. Bourhis, J. Hall, J.-J. Fontaine, M.-C. Vozenin, Ultra high dose-rate FLASH irradiation increases the differential response between normal and tumor tissue in mice, Sci. Transl. Med. 16 (2014) 1–9.

[2] P. Montay-Gruel, K. Petersson, M. Jaccard, G. Boivin, J.-F. Germond, B. Petit, R. Doenlen, V. Favaudon, F. Bochud, C. Bailat, J. Bourhis, M.-C. Vozenin, Irradiation in a flash: unique sparing of memory in mice after whole brain irradiation with dose rates above 100 Gy/s, Radiother. Oncol. 124 (2017) 365–369.

[3] J. Bourhis, W.J. Sozzi, P.G. Jorge, O. Gaide, C. Bailat, F. Duclos, D. Patin, M. Ozsahin, F. Bochud, J.-F. Germond, R. Moeckli, M.-C. Vozenin, Treatment of a first patient with FLASH-radiotherapy, Radiother. Oncol. 139 (2019) 18–22.

[4] E. Schuler, S. Trovati, G. King, F. Lartey, M. Rafat, M. Villegas, A.J. Praxel, B.W. Loo, P.G. Maxim, Experimental platform for ultra-high dose rate FLASH irradiation of small animals using a clinical linear accelerator, Int. J. Radiat. Oncol. Biol. Phys. 97 (2017) 195–203.

[5] M. Lempart, B. Blad, G. Adrian, S. Back, T. Knoos, C. Ceberg, K. Petersson, Modifying a clinical linear accelerator for delivery of ultra-high dose rate irradiation, Radiother. Oncol. 139 (2019) 40–45.

[6] L.G. Marcu, E. Bezak, D.D. Peukert, P. Wilson, Translational research in FLASH radiotherapy—from radiobiological mechanisms to in vivo results, Biomedicines 9 (2021) 1–15.

[7] H. Lim, D.H. Jeong, K.W. Jang, S.K. Kang, H.C. Kim, S.H. Kim, D.E. Lee, K.H. Lee, S.J. Lee, M. Lee, Implementation of ultra-high dose-rate electron beam from 6-MeV C-band linear accelerator for preclinical study, J. Instrum. 15 (2020), P09013.

[8] K. Petersson, M. Jaccard, J.-F. Germond, T. Buchillier, F. Bochud, J. Bourhis, M.-C. Vozenin, C. Bailat, High dose-per-pulse electron beam dosimetry—a model to correct for the ion recombination in the Advanced Markus ionization chamber, Med. Phys. 44 (2017) 1157–1167.

[9] J.W. Boag, E. Hochhauser, O.A. Balk, The effect of free-electron collection on

the recombination correction to ionization measurements of pulsed radiation, Phys. Med. Biol. 41 (1996) 885–897.
[10] R.F. Laitano, A.S. Guerra, M. Pimpinella, C. Caporali1, A. Petrucci, Charge collection efficiency in ionization chambers exposed to electron beams with high dose per pulse, Phys. Med. Biol. 51 (2006) 6419–6436.
[11] D.H. Jeong, M. Lee, H. Lim, S.K. Kang, K.W. Jang, High-dose-rate electron-beam dosimetry using an advanced Markus chamber with improved ion-recombination corrections, Prog Med Phys 31 (2020) 145–152.
[12] T.C. Zhu, I.J. Das, B.E. Bjarngard, Characteristics of bremsstrahlung in electron beams, Med. Phys. 28 (2001) 1352–1358.
[13] F.H. Attix, Introduction to Radiological Physics and Radiation Dosimetry, John Wiley & Sons, Inc., New York, 1986, pp. 177–178.
[14] https://physics.nist.gov/PhysRefData/Xcom/html/xcom1.html.
[15] D.H. Jeong, M. Lee, H. Lim, S.K. Kang, S.J. Lee, H.C. Kim, K. Lee, S.H. Kim, D.E. Lee, K.W. Jang, Electron beam scattering device for FLASH preclinical studies with 6-MeV LINAC, Nucl. Eng. Technol. 53 (2021) 1289–1296.
[16] P. Andreo, D.T. Burns, K. Hohlfeld, M.S. Huq, T. Kanai, F. Laitano, V. Smyth, S. Vynckier, Absorbed Dose Determination in External Beam Radiotherapy: an International Code of Practice for Dosimetry Based on Standards of Absorbed Dose to Water, International Atomic Energy Agency, 2006, pp. 150–151. IAEA TRS-398.
[17] F.M. Khan, The Physics of Radiation Therapy, Lippincott Williams and Wilkins, Philadelphia, pp 106-155.
[18] Elsa Y. León Marroquin, A. José, González Herrera, A. Miguel, Camacho López, E. José, Villarreal Barajas, A. Olivia, García-Garduño, Evaluation of the uncertainty in an EBT3 film dosimetry system utilizing net optical density, J. Appl. Clin. Med. Phys. 17 (2016) 466–481.